Journal of Medical Systems (2019) 43: 252
https://doi.org/10.1007/s10916-019-1396-0

IMAGE & SIGNAL PROCESSING

An Efficient Method for the Detection of Oblique Fissures from Computed Tomography images of Lungs

S Anitha [1] · T R Ganesh Babu [1]

Received: 12 March 2019 / Accepted: 18 June 2019 / Published online: 28 June 2019

Abstract
Detection of a pulmonary fissure in lungs is difficult due to its anatomical changeability among humans and it is essential in the clinical environment for accurate localizing and treating the lung abnormalities on a lobe level in human lungs. In this work, an algorithmic approach is proposed to detect the lung oblique fissures from lung computed tomography (CT) images. In the preprocessing module of our approach, the lung structures are enhanced using morphological operation and lung images are de-noised using Wiener filter. In the second module, lung regions are segmented using techniques, namely, thresholding and background subtraction. In the third module of our algorithm, initially, fissure regions are segmented using the active contour model, then by applying the rule based approach on the fissure regions, the oblique fissures are segmented. The proposed algorithm has been tested on 50 images collected from Lung Image Database Consortium (LIDC) and 30 images obtained from Early Lung Cancer Action Program (ELCAP).

Keywords Segmentation · Lungs · Computed tomography (CT) images · Oblique fissure

Introduction

The importance of medical imaging in clinical applications is to visualize, analyze the human anatomy and for identifying the various diseases. CT is a powerful tool among other medical imaging techniques in capturing three dimensional bio-images [1]. CT produces voluminous of data and providing detailed structural (anatomical) information, it is the preferred imaging modality for assessing and localizing the lung disease [2]. Figure 1 describes the human lungs anatomy and the lungs have five different partitions called lobes and the boundaries of each lobe are fissures. The left lung has two lobes namely upper and lower lobe. The left oblique fissure separates the upper lobe from the lower lobe. There are three lobes in right lung namely upper, middle and lower lobe, in which the horizontal fissure divides the upper lobe from the middle lobe. The oblique fissure from the right lung divides the middle lobe from the lower lobe [3]. Fissures can visually appear as a sharp edge in high- resolution CT images and as a void space in clinical CT images where no vascular or bronchial trees cross each other [4]. In medical applications, lobar level analysis of the lung is appropriate for accurately locating and treating the disease within the lobar region. As the number of CT slice per CT scan is more than 200 slices in thin-section CT images, the fissure detection by the medical physician is tedious and time-consuming in the busy medical environment. Therefore, there is the prerequisite to develop a automatic methodology for the detection of fissure in lung images.

This article is part of the Topical Collection on *Image & Signal Processing*

✉ S Anitha
anithasep1983@gmail.com

T R Ganesh Babu
ganeshbabutr@gmail.com

[1] Department of Electronics and Communication Engineering, Muthayammal Engineering College, Rasipuram, Tamil Nadu, India

Literature survey

Numerous research works related to automatic or semi-automatic segmentation of fissures have been developed. These methods are primarily based on the concept of using lungs anatomical and grayscale information.

Zhou et al. [5], in their method have used both the anatomical information and statistical intensity distribution of lung structures to segment airway tree, lungs, fissures and lung

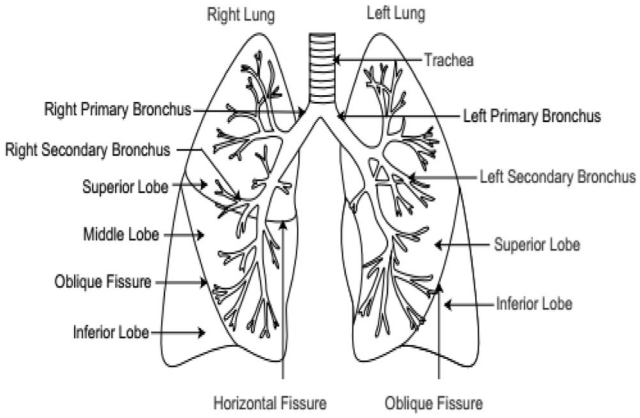

Fig. 1 Anatomy of human lungs

lobes from CT images. They have tested their method on 44 chest CT images and obtained a coincidence degree of 98% for lobar regions and an average shortest Euclidean distance of 1.8 mm–2.8 mm for fissure segmentation.

In Wang et al. [6], they have applied initialization step to identify the fissure key sections. In the next step, they have applied ridge map transformation to enhance the fissure. In the final step, they have applied the shape-based curve growing method to segment the lung boundary called fissure, in which the energy function is determined based on the Bayesian estimation theory. They have tested their method on 10 CT images with pulmonary nodules and obtained an average distance of 1.01 mm between their automatic methods with ground truth value.

In Wei et al. [7], in the first stage, they have applied fissure sweeping method to identify the fissure region. In second stage, they have used watershed transform to localize the locations and curvatures of the fissures in the fissure region. They have tested their method on six clinical CT images of thickness range from 2.5 mm–7 mm and achieved an accuracy of 85.5–95.0 for the oblique fissure in the left lung, 88.2–92.3 and 100% for an oblique fissure and horizontal fissure in the right lung respectively.

In Wei et al. [8], initially they have the applied sweeping technique to identify the fissure region. Finally, they have used wavelet operation to detect the fissure locations and curvatures in fissure region. They have tested their algorithm on 9-high resolution lung CT images of thickness 0.6 mm and achieved an accuracy of 76.7% for oblique fissure in the left lung, and 94.8% for horizontal fissure in the right lung.

In Pu et al. [9], they have used the shape property of the pulmonary fissure and it involves four steps, namely, lung region detection, binarization, initial fissure identification and fissure extension. They have evaluated their method on ten chest CT images with 0.625 mm thickness and obtained a root mean square (RMS) of 1.48 ± 0.92 to 2.04 ± 3.88.

In Ukil et al. [10], they have applied watershed transform followed by the graph search method to detect the complete fissure and have applied the fast marching method to identify the incomplete fissure. They have evaluated their method on 29 chest CT images and obtained a RMS error of less than 2.7 mm for all images.

In Wei et al. [11], have applied the Wiener filter to denoise the lung CT image. Then they have used the thresholding to detect the lung region. In the next step, they have applied texture analysis and feed forward

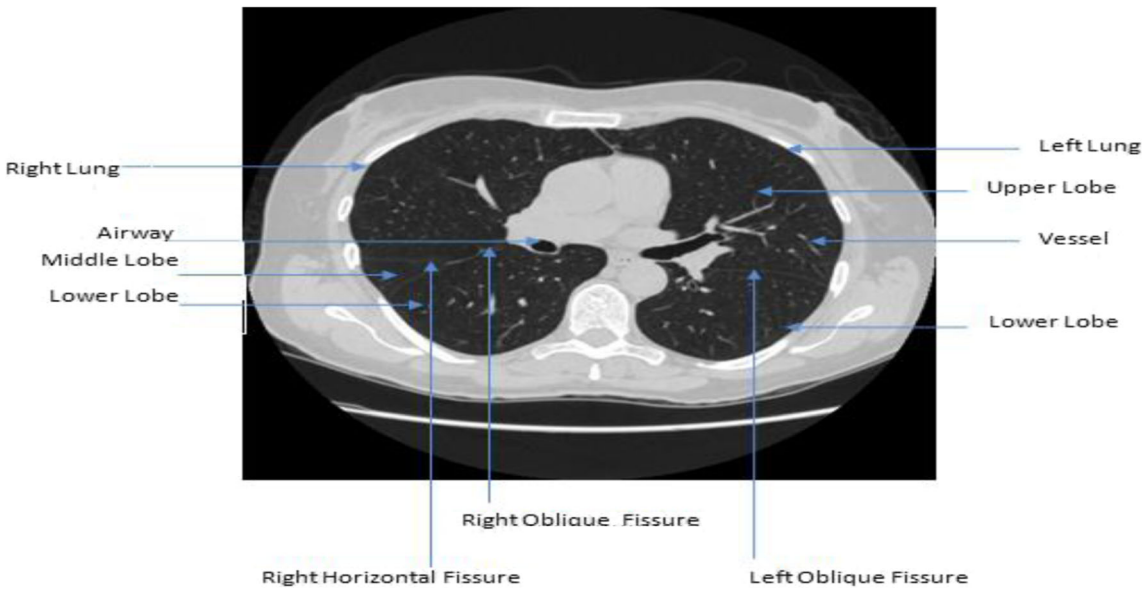

Fig. 2 Input Lung CT image

Neural Network to identify the fissure region. Finally, they have used the dynamic programming technique to detect the pulmonary fissure. They have tested their method on sixteen CT images of different pathologies and have validated their method with manual segmentation and obtained a mean distance of 1.92 ± 2.07 mm for oblique fissure in the left lung and 2.07 ± 2.37 mm for the oblique fissure in the right lung.

Gu et al. [12], in their method have applied the plane fitting method to detect the fissure patch and have used the clustering technique to classify the fissure into three types, namely, oblique fissure of the left lung, oblique fissure and horizontal fissure of the right lung. They have tested their method on 30 CT images of normal healthy case and different pathology cases. Compared with the manual segmentation, their approach obtained an RMS of 2.5 ± 3.3, mean of 1.0 ± 1.2 and the maximum distance of 20.5 ± 8.4 for the fissures namely oblique and horizontal fissures in the left and right lung.

Lassen et al. [13], in their work have the applied the thresholding method followed by morphological operation to segment the lung region. They have applied thresholding method and connected component analysis to segment the pulmonary vessels. In the next step, their approach has used the Hessian matrix technique to enhance the fissure and the fissures are detected based on mask construction and connected component technique. They have used the region growing method to segment the bronchi. The segmented vessels, fissures, and bronchi are integrated to form the cost image. Finally, they have used watershed transform on the cost image to segment the lung lobes. They have evaluated their algorithm on two datasets consisting of images of both normal and with pathological cases. For dataset 1 consisting of 20 CT scans, the algorithm obtained an average distance of 0.69 for the major fissure of the left lung, 0.67 for major fissure of the right lung and 1.21 for the minor fissure of the right lung. For dataset 2 consisting of 55 CT scans, the algorithm obtained an average distance of 0.98 for the major fissure in the left lung, 3.97 for the major fissure in the right lung, 3.09 for minor fissure in the right lung.

In Qi et al. [14], Initially, they have the applied fissure scanning technique to identify the fissure regions. They have used Hessian concept to enhance the fissure lines. Then they have used the cost search method to detect the fissure surfaces. They have applied three implicit fitting functions to segment the lung lobes. They have evaluated the method on a dataset consisting of fourteen images with mild emphysema and obtained a mean ± Standard Deviation of 2.05 ± 1.80 for the oblique fissure, 2.77 ± 2.12 for the horizontal fissure in the right lung, and 2.31 ± 1.76 for the oblique fissure in the left lung. The RMS values were 2.46 for the oblique fissure, 3.13 for the horizontal fissure in the right lung and 3.25 for the oblique fissure in the left lung.

Yu et al. [15], in their approach initially applied the thresholding method followed by the morphological rolling ball operation for segmenting the lung. Then they have used Hessian matrix concept to increase the intensity of the plane-like structures in the lung. Then they have used the local bending degree to detect the fissure surfaces. Then they have applied the maximum bending

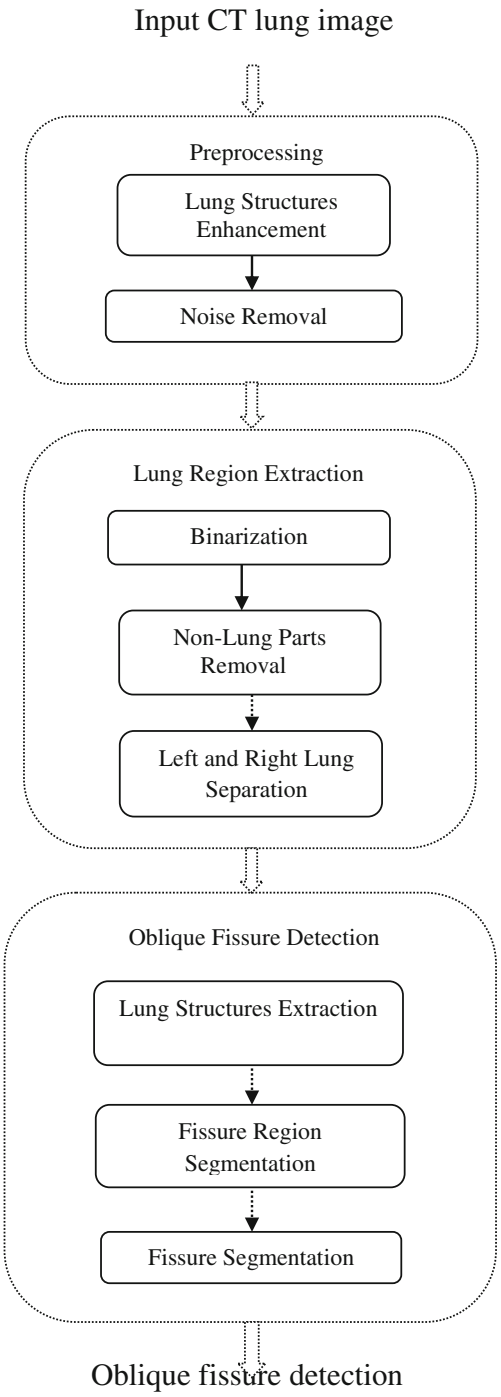

Fig. 3 Workflow of lung oblique fissure segmentation

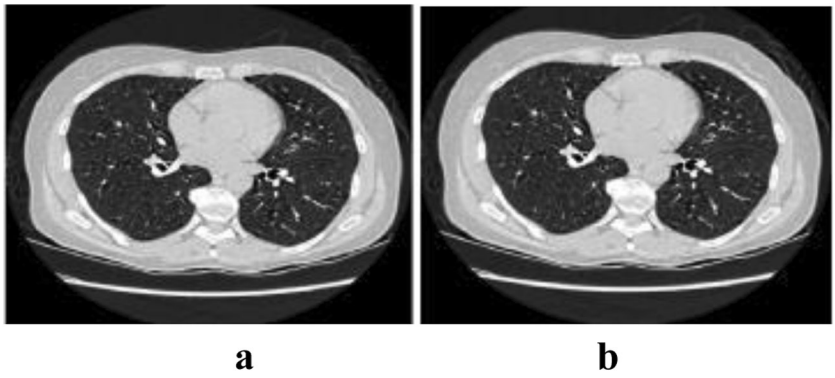

Fig. 4 Experimental results of preprocessing phase of proposed algorithm on a sample CT image from LIDC dataset. a. Lung structures enhanced Image b. Noise filtered image

degree to identify the fissure. Finally, they have applied the plane fitting method to fill the gaps present in identified fissure. They have evaluated their method on 15 chest CT images. Compared with the manual method, their approach obtained a mean value of the positive predictive value of 91%, sensitivity of 88%, the RMS distance of 1.01 ± 0.99, and the maximal RMS of 11.56 mm for fissure segmentation.

In Wei et al. [16], initially, they have applied the Wiener filter to de-noise the input image. To segment the oblique fissure, their method has applied the texture analysis using a neural network. Their method utilized the stack rotation followed by dynamic programming to segment the horizontal fissure. Finally, their algorithm applied the surface modeling technique to obtain a 3D view of lobes. They have tested the method on 24 lung images and obtained the RMS errors of 2.21 ± 1.21 for oblique fissure in the left lung, 2.51 ± 1.36 for oblique fissure in the right lung, and 2.38 ± 1.27 for the horizontal fissure in the right lung.

Xiao et al. [17] have proposed an approach for fissure segmentation. They have designed the derivative of stick filter based on the rotating kernel transformation to enhance the fissure. In the next stage, their method has utilized the multi-thresholding technique followed by steps, namely, branch point removal, and connected component analysis to segment the pulmonary interlobar fissure. They have evaluated their method on two datasets, namely, Lung and Lobe Analysis (LOLA11), which contains 55 CT images and Groningen and Leiden Universities, study of Corticosteroids in Obstructive Lung Disease (GLUCOLD) dataset which contains 23 CT images. Compared with the manual method, their algorithm have obtained a median-score of 0.833, 0.885 and 0.856 for left and right lungs separately from GLUCOLD dataset, and the combined left and right lungs from the LOLA11 dataset, respectively.

In Bragman et al. [18], initially, lungs, vessels and airways trees are segmented. Using auxiliary tree structures as anatomical information, the fissures were segmented. The segmented fissures were combined to construct the fissure model. The segmented fissures, anatomical information, and fissure model are then combined to obtain a cost image. Finally, lung lobes were segmented using the watershed segmentation method. They have evaluated their method on two datasets, namely, LOLA11 that contains 55 CT scans and Chronic Obstructive Pulmonary Disease (COPD) Gene study consisting of 30 CT scans. This method has obtained a F1-score of 0.90 for fissure segmentation in COPD dataset and the highest score of 0.884 for lobe segmentation in the LOLA1 dataset.

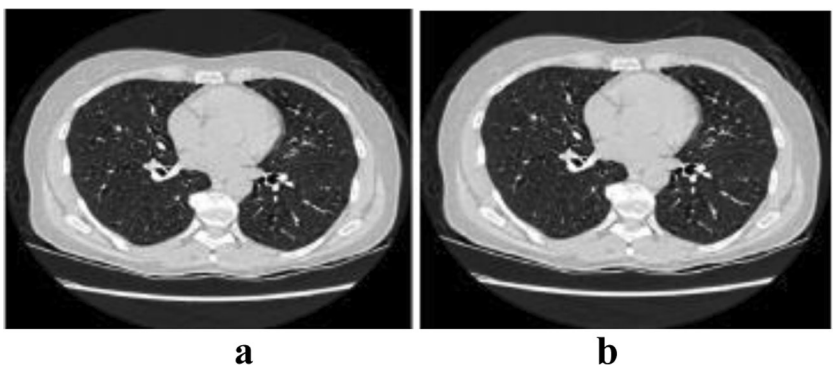

Fig. 5 Experimental results of preprocessing phase of proposed algorithm on a sample CT image from ELCAP dataset. a. Lung structures enhanced Image b. Noise filtered image

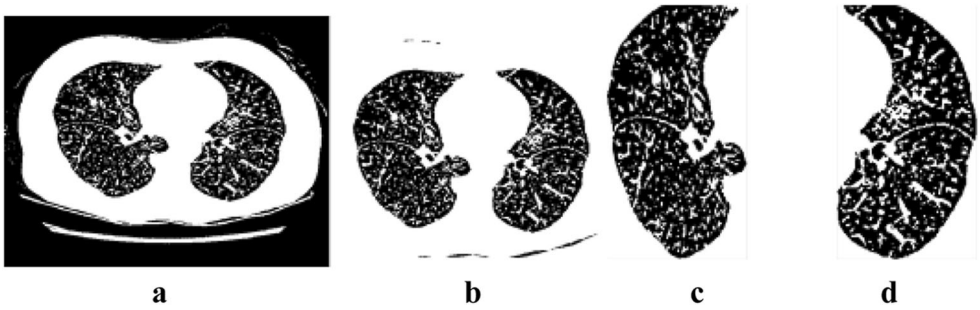

Fig. 6 Experimental results obtained from lung region extraction phase of proposed algorithm on a sample CT image of LIDC dataset. a. Thresholded image b. Lung region image c. Right lung image d. Left lung image

In George et al. [19], the algorithm have applied progressive holistically-nested network model to identify the lung fissures and used the random walker method to segment the lung lobes. They have tested their method on the Lung Tissue Research Consortium (LTRC) dataset consisting of 154 CT scans and obtained Jaccard score of 0.888 ± 0.164 to segment the lung lobes.

In Giuliani et al. [20], they have used both anatomical and prior shape knowledge to segment the lung lobes. They have evaluated their method on two datasets namely, the in-house dataset that contains 25 CT scans and LOLA11 dataset consisting of 55 CT scans. For the in-house dataset, the algorithm has obtained a median absolute distance of 1.04 mm and for the LOLA11 dataset the algorithm obtained a score of 0.866.

Devaki and Bhaskaran [21] have proposed an approach to segment the fissure from lung CT images. In their work, they have applied a watershed method to detect the region consisting of the fissure and non-fissure regions. Finally they have applied removal method to remove the accessory fissure and non-fissure region. They have evaluated their method on six CT scans of normal and pathology and obtained an RMS of 0.877 ± 0.224 for the oblique fissure in the left lung and 0.803 ± 0.262 for the oblique fissure in the right lung.

In the proposed approach, a segmentation approach is employed to detect the oblique fissure from left and right lung. The approach has used both the anatomical and grayscale information of the lung for efficient detection of the pulmonary fissure from lung CT images.

Contribution of the proposed algorithm

The proposed segmentation approach is different from other work in the following aspect

- The morphological algorithm applied in preprocessing module enhances the structures of the lung, namely, fissures, bronchial and vascular trees and thereby the algorithm accurately localizes the fissure region.
- Rule-based approach in the oblique fissure detection phase efficiently detects the oblique fissure.

The rest of the paper is organized as follows: In section "Materials and methods", the materials and methods for the proposed segmentation algorithm is given in detail. Results and discussion about the proposed algorithm are given in section "4 and 5" and in the last section, conclusion are made.

Materials and methods

The proposed work aims at developing an efficient model to detect the lung fissure from lung computed tomography (CT) images. The input CT lung image is presented in fig. 2 where the fissures, vessels, lobes are marked by blue arrows. The detailed workflow is shown in fig. 3. The work involves three modules. The modules are pre-processing, lung region extraction and oblique fissure detection. In the pre-processing module, the lung structures

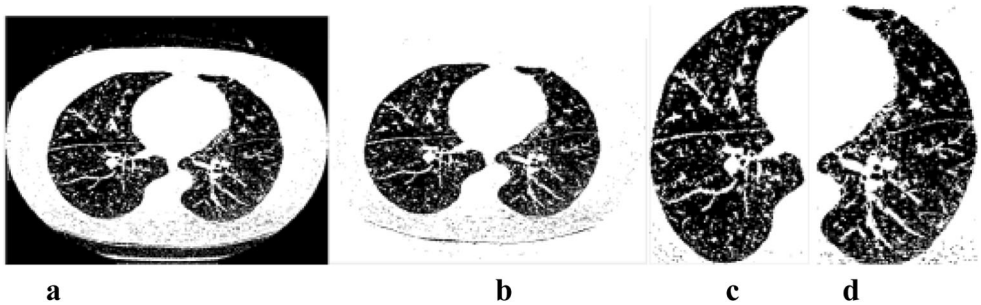

Fig. 7 Experimental results obtained from lung region extraction phase of proposed algorithm on a sample CT image of ELCAP dataset. a. Thresholded image b. Lung region image c. Right lung image d. Left lung image

(fissures, vascular and bronchial trees) are enhanced and the lung image is filtered. In lung region extraction module, preprocessed lung image is binarized, non-lung parts are removed and finally the left lung separated from the right lung. In the oblique fissure detection process, the structures of the lung are enhanced and segmented, the fissure regions are segmented using the contour model, the fissure region are enhanced, finally, the left and right oblique fissures are segmented from the fissure region.

Pre-processing

This stage consists of two sub-processes performed on the CT image, which include lung structures enhancement and noise removal. In lung enhancement, the lung structures, namely, the fissures, vascular and bronchial trees are enhanced using morphological transformation technique. In the noise-removal process, the noise in the CT lung image is filtered using the Weiner filter.

Lung inner structures enhancement

As the fissures appear as straight line which originate from outside boundary to inside boundary of the lungs and it appear only in the region absence of bronchial and vascular trees. The proposed algorithm uses this anatomical information to accurately locates fissure regions more efficiently. Therefore it is necessary to enhance the bronchial and vascular tress. The fissures, bronchial and vascular trees in the lung CT image are enhanced using the morphological algorithm [22, 23]. This algorithm uses top-hat operation and bottom-hat operation. In top-hat operation, the morphological opening of the input image with the structural element is subtracted from the input image and is mathematically represented in Eq. 1. In bottom- hat operation, the morphological closing of the input image with the structural element is subtracted from the input image and is mathematically represented in Eq. 2.

$$Top{-}HatTransFormed\mathrm{Image}(T_h) = I_I{-}(I_I \circ S_E) \tag{1}$$

$$Bottom{-}HatTransFormed\mathrm{Image}(B_h) = I_I{-}(I_I \bullet S_E) \tag{2}$$

Where I_I represents the input image, S_E represents the structuring element, $\circ$ represents the opening operation, and $\bullet$ represents the closing operation.

Algorithm 1 Lung inner Structures Enhancement

Input: CT lung image

Output: Lung structures enhanced image

Steps:

1. Perform top-hat and bottom-hat operation on input CT lung image
2. Add the original input with the top-hat image and the resultant output (C_T) is represented in Equation 3.

$$C_T = T_h + I_I \tag{3}$$

3. Subtract the bottom-hat transformed image from the image (C_T) and the resultant image (R_T) is given in Equation 4.

$$R_T = C_T - B_h \tag{4}$$

Noise removal

The random noise in CT scanners limits the radiologist's capability in discriminating two regions of different density in CT images [24]. This type of noise can be modeled as Gaussian distribution. Wiener filter is more appropriate to de-noise the Gaussian noise in lung image [25]. Wiener filter finds that the estimate of the input image such that the mean square error is minimized [26].

Lung region extraction

The other parts such as fat and muscles outside the lung are removed in order to limit the search to lung structures inside the lung. This phase consists of following sub-processes, namely, binarization, and elimination of non-lung parts and separation of left and right lung.

Binarization

The global thresholding technique [27] is used to transform the preprocessed grayscale lung image into a binary output. The histogram is computed for the preprocessed image and valley point from the histogram is used as the threshold value [28].

Algorithm 2 Binarization

Input: Preprocessed lung image
Output: Thresholded image
Steps:

1. Select the threshold value from the image histogram.
2. The pixels value greater than or equal to the threshold are replaced by one and the pixels value less than the threshold are replaced by zero.

Non-lung parts removal

Morphological flood-filling operation followed by background subtraction is used to remove the regions outside the region of interest (lung region). In the flood-filling operation, the holes in the input image are filled till it reaches the object boundary to make the background pixel values equal to the foreground pixel values.

Algorithm 3 Non-lung parts removal

Input: Thresholded binary image
Output: Region of interest image
Steps:

1. Apply morphological flood-filling operation on the input image.
2. Perform background subtraction of the binary image from the filled image to get the region of interest.

Left lung and right lung separation

Performing connected component analysis followed by feature analysis on the lung image, the left and right lungs are separated from each other.

Algorithm 4 Separation of Left and Right Lung

Input: Region of interest (Lung image)
Output: Left lung image and right lung image
Steps:

1. Perform connected component analysis based on four neighbour connectivity on the input image to label the connected components in the image.
2. Extract the features on the labeled image, namely, area, bounding box.
3. Bounding box is created for the region only if the region area greater than 5500.
4. Crop the lung image into left and right lung separately.

Oblique fissure detection

In this phase, initially the lung structures are enhanced and segmented, the fissure regions are segmented and finally, the oblique fissures are detected on the fissure region image.

Lung inner structure extraction

Lung structures are enhanced using morphological algorithm as discussed in preprocessing of the proposed work. The lung structures are extracted using background subtraction.

Fissure region segmentation

In this phase, region of interest (vessels and fissure) are segmented. Since fissure region contains vessels and fissures, in which both fissure and vessels appear as continuous or discontinuous bright line in CT image, the Chan-Vese active contour model is more suitable for segmenting the region of interest. This model depends on global properties of the image namely gray level intensities, contour length, region areas instead of gradient of the image and detects the complex objects namely holes, contour and disconnected regions. This method relies on the concept of computation of minimal energy path is mathematically represented in Eq. 5 [29, 30]. The starting position of the contour and maximum iteration is specified to start the curve to grow in the fissure regions.

$$G(b1,b2,b) = A.length(x) + S.Area(x) + \lambda_1 \int_{inside(b)} |\mu_0\left(x,y\right)b_1|^2 + \lambda_2 \int_{outside(b)} |\mu_0(x,y)b_2|^2 \quad (5)$$

Where $\mu_0(x,y)$ represents the input image, b represents the growing curve λ_1 and λ_2 are positive constant parameters and value equal to one, b_1 and λ_2 are intensity level inside and outside the contour b, A represents the parameter controls the length of the contour and S represents the parameter controls the area inside the contour.

The minimization problem is represented as,

$$\inf_{b1,b2,b} G(b1,b2,b) \quad (6)$$

Fissure segmentation

In this phase within the segmented fissure region, the oblique fissures are segmented in the lung image. Initially Morphological dilation operation as discussed in preprocessing of the proposed algorithm is applied to enhance the fissure region. As the fissure visually appears as a sharp line in lung CT images, line-type structuring element length one and degree zero is chosen based on the experimental analysis. Then Connected component technique of four neighbour connectivity is applied to identify the connected components of the fissure region. In rule based approach, major axis length is measured for all the labeled connected components in the fissure

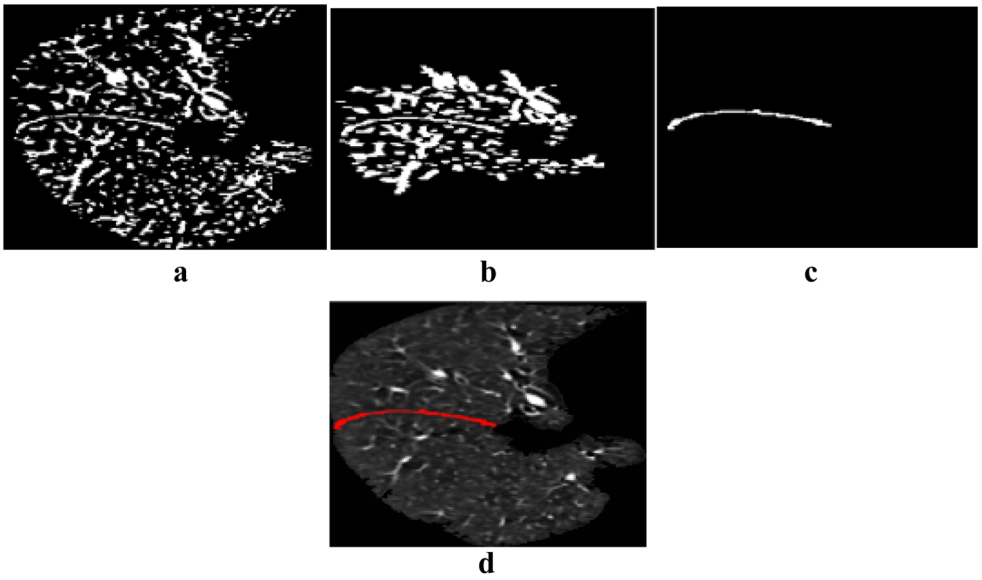

Fig. 8 Experimental results of right lung fissure detection phase of proposed algorithm on a sample CT image from LIDC dataset a. Lung structures enhanced image b. Fissure region segmented image c. Oblique fissure segmented image d. Oblique fissure detected image

region, then the fissure is detected based on maximum major axis length of the connected component in the fissure region.

$$ed_i = \min_j \sqrt{\left(X_{aj} - X_{mi}\right)^2 + \left(Y_{aj} - Y_{mi}\right)^2} \tag{7}$$

$$Mean = \frac{\left(\sum_{i=1}^{n} ed_i\right)}{n} \tag{8}$$

$$RMSE = \frac{\sqrt{\sum_{i=1}^{n} ed_i^2}}{n} \tag{9}$$

$$SD = \sqrt{\frac{1}{n}\left(\sum_{i=1}^{n} \left(ed_i - ed_{mean}\right)^2\right)} \tag{10}$$

$$Max = \max_i \left(ed_i\right) \tag{11}$$

Evaluation metrics for fissure validation

Compared with the manual method, the accuracy of the proposed approach is calculated using the parameters [10, 14] namely, Euclidean distance (ed), mean of the euclidean distance (Mean), standard deviation of the euclidean distance (SD), root mean square error (RMSE) and maximum of the euclidean distance (Max) is represented mathematically in Eqs. 7, 8, 9, 10 and 11.

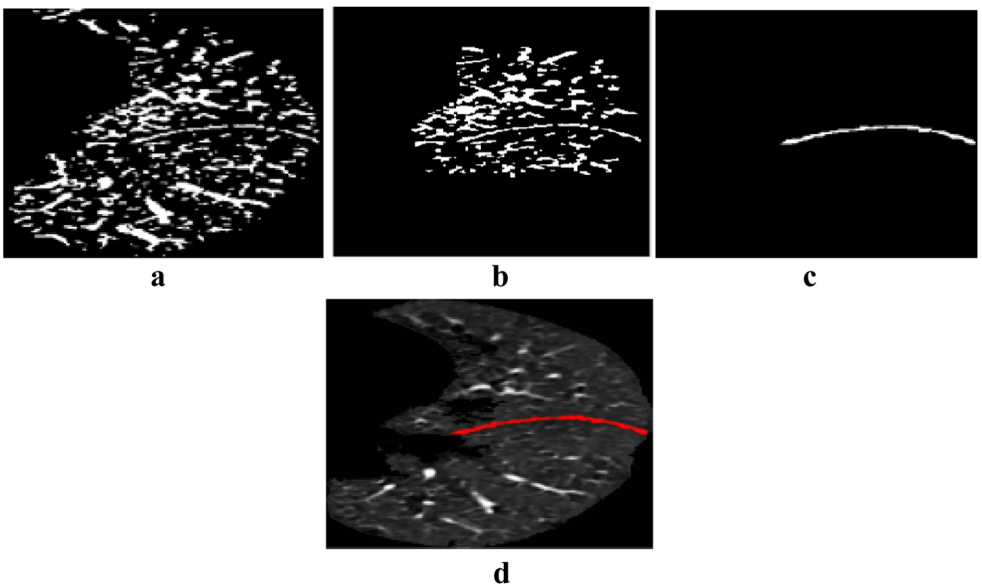

Fig. 9 Experimental results of left lung fissure detection phase of proposed algorithm on a sample CT image from LIDC dataset. a. Lung structures enhanced image b. Fissure region segmented image c. Oblique fissure segmented image d. Oblique fissure detected image

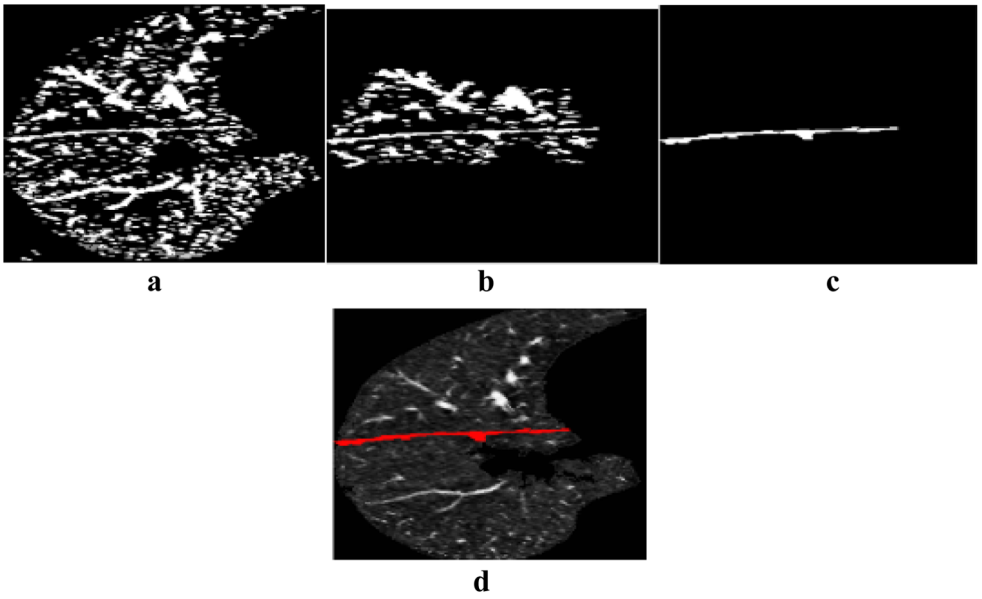

Fig. 10 Experimental results obtained from right lung fissure detection phase of proposed algorithm on a sample CT image of ELCAP dataset. a. Lung structures enhanced image b. Fissure region segmented image c. Oblique fissure segmented image d. Oblique fissure detected image

Where (X_a, Y_a) and (X_m, Y_m) are the corresponding pixel coordinates of the automatic and manual segmented result.

Results

The proposed algorithm are implemented using Mat Lab 2014 and tested on 30 low-dose lung CT scans of 1.5 mm thickness taken from ELCAP database and 50 lung CT scans of 1.5 mm thickness and 2.5 mm from LIDC database.

In preprocessing module, initially lung inner structures are enhanced using morphological algorithm, in which the disk type structuring element of size 6*6 is chosen based on repeated experimental analysis to yield accurate results. The resultant lung inner structures enhanced image for a sample CT image from LIDC dataset is given in Fig. 4a and for a sample CT image from ELCAP dataset is given in fig. 5a. The noise in LIDC dataset is less compared to ELCAP dataset and based on repeated experimental analysis, the filter of size 2*2 is chosen as optimum in case of LIDC dataset and 3*3 is chosen for ELCAP dataset and the resultant de-noised image for a sample CT image from LIDC dataset is shown in fig. 4b and for a sample CT image from ELCAP dataset is given in fig. 5b.

In lung region extraction module, initially thresholding is applied to transform gray scale image to binary image. The threshold value from the histogram is chosen based on repeated experimental analysis and the values are 55 for CT images of 1.5 mm thickness, 90 for CT images of 2.5 mm thickness. The resultant binary image for a sample CT lung image from LIDC dataset is shown in fig. 6a, and for sample CT lung

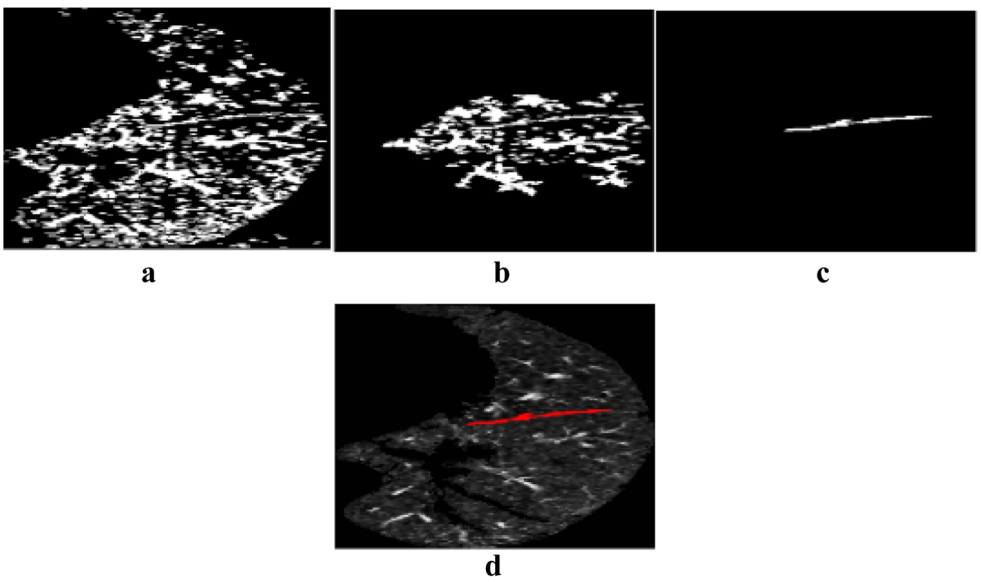

Fig. 11 Experimental results obtained from left lung fissure detection phase of proposed algorithm of ELCAP dataset. a. Lung structures enhanced image b. Oblique fissure region segmented image c. Oblique fissure segmented image d. Oblique fissure detected image

Table 1 Initial contour location and iteration values

Database	Iteration	Seed point for left lung	Seed point for right lung
LIDC	500	(50:18,44:32)	(83:177,7:140)
ELCAP	500	(116:194,50:164)	(97:187,13:132)

image from ELCAP dataset is shown in fig. 7a. Morphological flood filling operation followed by background subtraction on the binary image, the non- lung parts are removed and the resultant lung region image for a sample CT lung image from LIDC dataset is shown in fig. 6b,and for a sample CT lung image from ELCAP dataset is shown in fig. 7b. After applying connected component analysis and feature analysis, the left and right lung are separated and the resultant right and left lung image from LIDC dataset is shown in fig. 6c and d. The resultant right and left lung image from ELCAP dataset is shown in fig. 7c and d.

In oblique fissure detection module, lung inner structures are extracted using morphological algorithm followed by background subtraction and the resultant lung inner structures extracted image for a sample CT right lung image from LIDC dataset is shown in fig. 8a. Figure 9a shows the resultant lung inner structures extracted image for a sample CT left lung image from LIDC dataset.

The resultant lung inner structures extracted image for a sample CT right lung image from ELCAP dataset is shown in fig. 10a. Figure 11a shows the resultant lung inner structures extracted image for a sample CT left lung image from ELCAP dataset. Chan-Vese active contour is applied to segment the fissure region and the contour position and iteration parameters are chosen based on repeated experimental analysis to accurately segment the fissure region and the values are given in Table 1.

The resultant fissure region segmented image sample CT right lung image from LIDC dataset is shown in fig. 8b. Figure 9b shows the resultant fissure region segmented image for a sample CT left lung image from LIDC dataset. The resultant fissure region segmented image for a sample CT right lung image from ELCAP dataset is shown in fig. 10b. Figure 11b shows the resultant fissure region segmented image for a sample CT left lung image from ELCAP dataset. By applying feature extraction and rule based technique on the fissure region, the oblique fissure is detected and the resultant right oblique fissure segmented image from LIDC dataset is shown in fig. 8c. Figure 9c shows the resultant left oblique fissure segmented image from LIDC dataset. The resultant right oblique fissure segmented image from ELCAP dataset is shown in fig. 10c. Figure 11c shows the resultant left oblique fissure segmented image from ELCAP dataset. The fissure segmented image is superimposed with original right lung image and the resultant right oblique fissure detected image from LIDC dataset is shown in 8d. Figure 9d shows the detected oblique fissure in the left lung image from LIDC dataset. The resultant oblique fissure detected in the right lung image from ELCAP dataset is shown in 10d. Figure 11d shows the detected oblique fissure in the left lung image from ELCAP dataset.

.

Discussion

In-order to validate our algorithm, automated fissure is statistically compared with manual segmented fissure. Table 2 represents the evaluating results of proposed algorithm for segmenting the left oblique and right oblique fissure in LIDC dataset. Table 3 represents the evaluating results of proposed algorithm for segmenting

Table 2 Fissure validation results for LIDC dataset

Patient No.	Left oblique fissure				Right oblique fissure			
	SD	Mean	RMSE	Max	SD	Mean	RMSE	Max
1	0.045	0.005	0.045	0.529	0.097	0.039	0.096	0.591
2	0.084	0.014	0.085	0.748	0.158	0.070	0.152	1.122
3	0.045	0.007	0.039	0.264	0.150	0.056	0.151	1.090
4	0.200	0.055	0.207	1.182	0.215	0.067	0.206	1.348
5	0.180	0.033	0.183	1.424	4.182	3.309	4.497	11.881
6	0.444	0.136	0.457	2.181	2.396	1.944	2.173	7.353
7	0.158	0.045	0.164	0.953	0.289	0.114	0.280	1.851
8	0.419	0.113	0.402	2.438	0.097	0.041	0.100	0.374
9	0.161	0.042	0.166	0.953	1.211	0.657	1.123	4.305
10	0.046	0.005	0.0466	0.529	0.100	0.044	0.104	0.374
Ave.(50 cases)	0.706	0.513	0.785	2.758	0.765	0.610	0.852	2.865

Table 3 Fissure validation results for ELCAP dataset

Patient No.	Left oblique fissure				Right oblique fissure			
	SD	Mean	RMSE	Max	SD	Mean	RMSE	Max
1	0.453	0.169	0.483	1.925	0.143	0.027	0.146	1.090
2	0.190	0.046	0.196	1.322	0.216	0.060	0.220	1.322
3	0.097	0.015	0.098	0.836	0.019	0.001	0.019	0.2645
4	0.432	0.139	0.453	2.275	0.099	0.012	0.100	0.836
5	0.038	0.005	0.038	0.264	0.068	0.010	0.068	0.529
6	0.247	0.086	0.261	1.182	0.079	0.009	0.079	0.836
7	0.270	0.050	0.274	2.065	0.800	0.267	0.761	5.088
8	0.132	0.039	0.138	0.954	2.105	1.670	2.107	6.106
9	0.086	0.032	0.092	0.264	0.414	0.122	0.4327	2.658
10	0.329	0.114	0.347	1.870	0.751	0.237	0.786	3.712
Ave.(30 cases)	0.333	0.127	0.359	1.825	0.747	0.394	0.805	3.334

the left oblique and right oblique fissure in ELCAP dataset. From the results of Table 2, it is inferred that, our proposed method obtained a less RMS error of 0.785, 0.852 mm for segmenting the left and right oblique fissure respectively for averaged overall 50 CT images of LIDC dataset. From the results of Table 3, it is inferred that, our proposed method obtained a less RMS error of 0.359, 0.805 mm for oblique fissure segmentation of left and right lung respectively for averaged overall 30 CT images of ELCAP dataset.

Conclusion

An algorithmic framework is developed for segmenting left and right oblique fissure on 30 lung CT images from ELCAP dataset and 50 lung CT images from LIDC dataset. In the preprocessing process, the noise in lung images is filtered using Wiener filter and the lung structures are enhanced using morphological algorithm. In next step, lung region are segmented using thresholding followed by background subtraction. Fissure region are identified using the Chan-vese active contour model. Finally, the oblique fissure is segmented using rule-based approach. The proposed work detects only the oblique fissure in the left and right lung and excludes the detection of horizontal fissure. The algorithm tested on 50 lung CT scans from LIDC dataset and obtained an RMS error of 0.785 for oblique fissure in the left lung and 0.852 for oblique fissure in the right lung. For the 30 CT scans from ELCAP dataset, the algorithm obtained an RMS error of 0.359 for oblique fissure in the left lung and 0.805 for oblique fissure in the right lung. The work can be further improved by segmenting both the horizontal and oblique fissure in normal and severe pathological cases.

References

1. Abbasi, H., Kavehvash, Z., and Shabany, M., Improved CT image reconstruction through partial Fourier sampling. Scientia Iranica: 2908–2916, 2016.
2. Dhawan, A. P., John Wiley and sons, *Medical image analysis*. Vol. 31, 2011.
3. Nene, A. R., Gajendra, K. S., and Sarma, M. V. R., Lung lobes and fissures: a morphological study. Anatomy 5(1), 2011.
4. Hayashi, K., Aziz, A., Ashizawa, K., Hayashi, H., Nagaoki, K., and Otsuji, H., Radiographic and CT appearances of the major fissures. Radiographics 21(4):861–874, 2001.
5. Zhou, X., Hayashi, T., Hara, T., Fujita, H., Yokoyama, R., Kiryu, T., and Hoshi, H., Automatic segmentation and recognition of anatomical lung structures from high-resolution chest CT images. Comput. Med. Imaging Graph. 30(5):299–313, 2016.
6. Wang, J., Betke, M., and Ko, J. P., Pulmonary fissure segmentation on CT. Med. Image Anal. 10(4):530–547, 2006.
7. Wei, Q., Hu, Y., MacGregor, J. H., and Gelfand, G., Segmentation of lung lobes in clinical CT images. Int. J. Comput. Assist. Radiol. Surg. 3(1–2):151–163, 2008.
8. Wei, Q., Hu, Y., Gelfand, G., and Macgregor, J. H., Segmentation of lung lobes in high-resolution isotropic CT images. IEEE Trans. Biomed. Eng. 56(5):1383–1393, 2009.
9. Pu, J., Leader, J. K., Zheng, B., Knollmann, F., Fuhrman, C., Sciurba, F. C., and Gur, D., A computational geometry approach to automated pulmonary fissure segmentation in CT examinations. IEEE Trans. Med. Imaging 28(5):710, 2009.
10. Ukil, S., and Reinhardt, J. M., Anatomy-guided lung lobe segmentation in X-ray CT images. IEEE Trans. Med. Imaging 28(2):202–214, 2009.
11. Wei, Q., Hu, Y., MacGregor, J. H., and Gelfand, G., Automatic recognition of major fissures in human lungs. Int. J. Comput. Assist. Radiol. Surg. 7(1):111–123, 2012.
12. Gu, S., Wilson, D., Wang, Z., Bigbee, W. L., Siegfried, J., Gur, D., and Pu, J., Identification of pulmonary fissures using a piecewise plane fitting algorithm. Comput. Med. Imaging Graph. 36(7):560–571, 2012.
13. Lassen, B., van Rikxoort, E. M., Schmidt, M., Kerkstra, S., van Ginneken, B., and Kuhnigk, J. M., Automatic segmentation of the pulmonary lobes from chest CT scans based on fissures, vessels, and bronchi. IEEE Trans. Med. Imaging 32(2):210–222, 2013.

14. Qi, S., van Triest, H. J., Yue, Y., Xu, M., and Kang, Y., Automatic pulmonary fissure detection and lobe segmentation in CT chest images. Biomed. Eng. Online 13(1):59, 2014.
15. Yu, M., Liu, H., Gong, J., Jin, R., Han, P., and Song, E., Automatic segmentation of pulmonary fissures in computed tomography images using 3D surface features. J. Digit. Imaging 27(1):58–67, 2014.
16. Wei, Q., and Hu, Y., A hybrid approach to segmentation of diseased lung lobes. IEEE Journal of Biomedical and Health Informatics 18(5):1696–1706, 2014.
17. Xiao, C., Stoel, B. C., Bakker, M. E., Peng, Y., Stolk, J., and Staring, M., Pulmonary fissure detection in CT images using a derivative of stick filter. IEEE Trans. Med. Imaging 35(6):1488–1500, 2016.
18. Bragman, F. J., McClelland, J. R., Jacob, J., Hurst, J. R., and Hawkes, D. J., Pulmonary lobe segmentation with probabilistic segmentation of the fissures and a groupwise fissure prior. IEEE Trans. Med. Imaging 36(8):1650–1663, 2017.
19. George, K., Harrison, A.P., Jin, D., Xu, Z. and Mollura, D.J., Pathological pulmonary lobe segmentation from ct images using progressive holistically nested neural networks and random walker. *In: Deep Learning in Medical Image Analysis and Multimodal Learning for Clinical Decision Support (Springer)* pp. 195–203, 2017.
20. Giuliani, N., Payer, C., Penn, M., Olschewski, H., and Urschler, M., Pulmonary Lobe Segmentation in CT Images using Alpha-Expansion. Proc. of VISIGRAPP:387–394, 2018.
21. Devaki, K., and Bhaskaran, V. M., A Novel Approach To Detect Fissures In Lung CT Images Using Marker-Based Watershed Transformation. J. Comput. Sci. 10(6):896, 2014.
22. Firoz, R., Ali, M. S., Khan, M. N. U., Hossain, M. K., Islam, M. K., and Shahinuzzaman, M., Medical image enhancement using morphological transformation. Journal of Data Analysis and Information Processing 4(01):1, 2016.
23. Quintanilla-Dominguez, J., Ojeda-Magaña, B., Cortina-Januchs, M. G., Ruelas, R., Vega-Corona, A., and Andina, D., Image segmentation by fuzzy and possibilistic clustering algorithms for the identification of microcalcifications. Scientia Iranica 18(3):580–589, 2011.
24. Hanson, K. M., Noise and contrast discrimination in computed tomography. Radiology of the Skull and Brain 5(1):3941–3955, 1981.
25. Darmanayagam, S. E., Harichandran, K. N., Cyril, S. R. R., and Arputharaj, K., A novel supervised approach for segmentation of lung parenchyma from chest CT for computer-aided diagnosis. J. Digit. Imaging 26(3):496–509, 2013.
26. Sridhar, S., Digital image processing. Oxford University Press, 2011.
27. Elaraby, A., and Moratal, D., A generalized entropy-based two-phase threshold algorithm for noisy medical image edge detection. Scientia Iranica:3247–3256, 2017.
28. Sharma, N., and Aggarwal, L. M., Automated medical image segmentation techniques. Journal of medical physics/Association of Medical Physicists of India 35(1):3, 2010.
29. Chan, T. F., and Vese, L. A., Active contours without edges. IEEE Trans. Image Process. 10(2):266–277, 2001.
30. Wang, X. F., Huang, D. S., and Xu, H., An efficient local Chan–Vese model for image segmentation. Pattern Recogn. 43(3):603–618, 2010.